Finite Element Modeling of SnAgCu Alloy on 3D Package-on-Package (POP) Subjected to Board Level Drop Test

Hsiang-Chen Hsu[*1], Shen-Wen Ju[2], Shih-Jeh Wu[3], Miin-Shyan Bair[4]

[1-3]Department of Mechanical and Automation Engineering, I-Shou University
[4]Department of Electronic Engineering, I-Shou University
No. 1, Section 1, Syuecheng Road, Dashu District, Kaohsiung City 84001, Taiwan, R. O. C.

[*1]hchsu@isu.edu.tw; [2]kublaja@yahoo.com.tw; [3]wsj007@isu.edu.tw; [4]bair@isu.edu.tw

Abstract

The objective of this research is to investigate the solder joint reliability of board-level 3D pyramid package-on-package (POP) stacked-die packages in transient drop analysis. Three kinds of lead-free solder alloy, Sn4Ag0.5Cu, Sn3.5Ag0.5Cu and Sn3.5Ag are introduced to demonstrate the transient dynamic response subjected to JEDEC sine wave pulse-controlled drop test. In order to evaluate the structure of the interested area a strip model sliced from, the full test vehicle is introduced in this research. In addition, the submodel region is particularly chosen with the strip model by performing the cut boundary interpolation. The envelope of equivalent stress for the outermost solder joint off the end of the strip model is drawn to illustrate the potential failure sites and mechanism. The cut boundary of submodel is verified and the mesh density of submodel is examined. For a refinery mesh of submodel, parametric studies for structure and material are carried out to investigate the reliability of the outermost solder joint, and the results are summarized as design rules for the development of 3D IC packages. A series of comprehensive parametric studies are conducted in this research.

Keywords

Solder Joint Reliability (SJR); Board-level Drop Test; Support Excitation Scheme; Submodel; Package-on-Package (POP)

Introduction

The tendency of advanced integrated circuit (IC) package techniques is characterized by lightness, thinness, small size and high performance. Hence, advance in the design and manufacture of the packaging technology need to keep pace with advance in the miniaturization of the electronic systems. The IC packaging technology plays an important role in determining the overall performance in the electronic system. The C4 (Controlled Collapse Chip Connection) packaging technique has been improved to ball grid array (BGA), flip chip (FC) and package-on-package (POP) technology in recent years [1-15]. In compliance with manufacturing process, the three dimensional (3D) packaging technique [1-2,4,7-9] presents the shortest leads with the minimized inductance as well as maximized frequency, and will become the leading packaging technologies in next generation0 There have been many 3D stack-die POP packaging structures reported [2-3] and developed for their easily compliance with the current manufacturing process.

The function of solder joints in the presented 3D POP structure are: electric interconnection, structural support and thermal conduction. In addition, the eutectic solder has been replaced by lead-free solder alloy in accordance with RoHS and WEEE environmental regulations. However, the primary difficulty encountered in these structures is the lead-free solder joints reliability (SJR) which is the probability of solder joints to perform their intended mechanical and electrical specifications over a given period of time and under a specified set of operating conditions. Four mechanisms of solder joint failure have been reported [13], such as tensile fracture due to mechanical overstress, creep failure caused by a permanent sustained load, fatigue resulted from a cyclic loading, and electronic migration owing to current crowding and working-temperature. Therefore, SJR studies, such as cycling temperature loading, electricity current crowding and transient drop effects, must take these failure mechanisms into consideration. SJR studies cover module-level and board-level solder joint reliability. Module-level SJR copes with the reliability of solder bumps within the package before board mounting. Board-level SJR deals with the reliability of solder joints on a package after board mounting. Board-level SJR for 3D POP package is

much more comprehensive because it comprises both the solder-to-package and solder-to-board interfaces.

Previous works [2-3] demonstrated that two categories of board-level drop tests, namely free drop test and pulse-controlled drop test, were developed to investigate the transient dynamic structural behavior of solder joints. In order to evaluate the solder joint reliability of on-board various electronic packages, the Joint Electronic Devices Engineering Council (JEDEC) proposed the pulse-controlled drop test regulations, JESD22-B104, JESD22-B110 and JESD22-B111, respectively. For packaging body size less than 15mm x 15mm, JESD22-B111 regulation of the half sine pulse of 1500G acceleration within 0.5ms duration time is the commonly used test standard in the field. Since board-level reliability testing is more difficult to implement, an alternative scheme to analyse solder joint strengths and weaknesses is finite element analysis (FEA) using computer models. Few methodologies, such as the response spectra analysis [7], the input G method [1] and the support excitation scheme [4-5], were developed to investigate the pulse-controlled board-level drop test effects. Many recent works [2-9] have been reported that the support excitation scheme produces no rigid-body motion to the test vehicle and dramatically reduces the computational cost.

The preliminary results show that the peak effective stress is located in the outermost solder joint off the end of strip model, which is the interesting region. Compared with the conventional numerical approach for drop tests, submodel technique provides both accurate and computationally economical solutions. Hence, the purpose of this research mainly concentrates on examining the transient dynamic response in the outermost solder ball for board-level drop tests based on the support excitation scheme.

Constitutive Model

Drop Test

Previous researches revealed drop tests were conducted by using KD-DP1200 drop apparatus. FIG. 1 demonstrates the drop test apparatus for the pulse-controlled board-level drop test based on JEDEC standard JESD22-B111. Detailed view of the drop system is schematic illustrated in FIG. 2, the drop table is freely released and along side guides from a certain altitude to hit the strike surface on the rigid base. The board-level test board is supported on the base plate with 4-corner fixed standoffs. Test board consists of fifteen representative samples bearing the solder joint of interesting POP stack-die packages. The base plate is welded on the drop table and the accelerometer is firmly attached to the base plate to monitor the peak acceleration and duration of half-sine impact pulse.

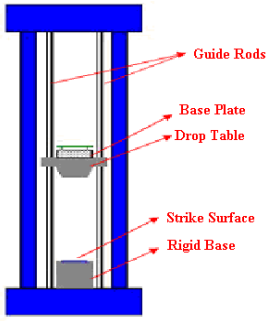

FIG. 1 SCHEMATICALLY ILLUSTRATION OF DROP TEST APPARATUS KD-DP1200

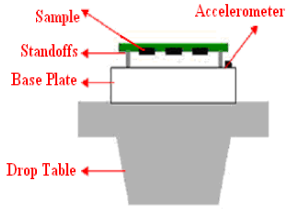

FIG. 2 DETAILED VIEW OF THE DROP SYSTEM

Support Excitation Scheme

Based on the support excitation scheme[4-5, 7-9], the drop test system presented in FIG. 2 can then be transferred into a multiple degree-of-freedom (MDOF) of mass-damper-spring time dependent vibration system. It should be noted that the origin of the coordinate system is located on the top surface of base plate where the accelerometer is attached. FIG. 3 depicts the corresponding MDOF time dependent vibration system.

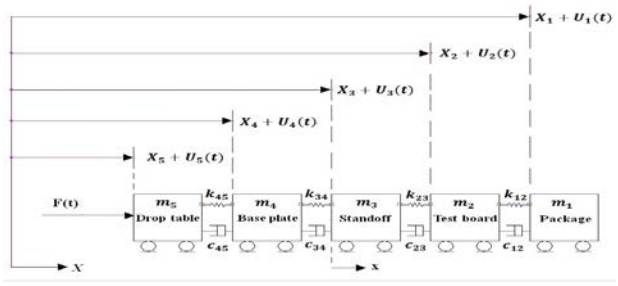

FIG. 3 MDOF OF MASS-DAMPER-SPRING TIME DEPENDENT VIBRATION SYSTEM FOR DROP SYSTEM IN FIG.2

In term of the force equilibrium along the X-direction on the MDOF system, equation of motion can be derived as follows

$$\begin{bmatrix} m_1 & 0 & 0 & 0 & 0 \\ 0 & m_2 & 0 & 0 & 0 \\ 0 & 0 & m_3 & 0 & 0 \\ 0 & 0 & 0 & m_4 & 0 \\ 0 & 0 & 0 & 0 & m_5 \end{bmatrix} \begin{Bmatrix} \ddot{U}_1 \\ \ddot{U}_2 \\ \ddot{U}_3 \\ \ddot{U}_4 \\ \ddot{U}_5 \end{Bmatrix} +$$

$$\begin{bmatrix} c_{12} & -c_{12} & 0 & 0 & 0 \\ -c_{12} & c_{12}+c_{23} & -c_{23} & 0 & 0 \\ 0 & -c_{23} & c_{23}+c_{34} & -c_{34} & 0 \\ 0 & 0 & -c_{34} & c_{34}+c_{45} & -c_{45} \\ 0 & 0 & 0 & -c_{45} & c_{45} \end{bmatrix} \begin{Bmatrix} \dot{U}_1 \\ \dot{U}_2 \\ \dot{U}_3 \\ \dot{U}_4 \\ \dot{U}_5 \end{Bmatrix} +$$

$$\begin{bmatrix} k_{12} & -k_{12} & 0 & 0 & 0 \\ -k_{12} & k_{12}+k_{23} & -k_{23} & 0 & 0 \\ 0 & -k_{23} & k_{23}+k_{34} & -k_{34} & 0 \\ 0 & 0 & -k_{34} & k_{34}+k_{45} & -k_{45} \\ 0 & 0 & 0 & -k_{45} & k_{45} \end{bmatrix} \begin{Bmatrix} U_1 \\ U_2 \\ U_3 \\ U_4 \\ U_5 \end{Bmatrix} = \begin{Bmatrix} 0 \\ 0 \\ 0 \\ 0 \\ F(t) \end{Bmatrix} \quad (1)$$

where m_i is the mass, U_i is the displacement, c_{ij} is the damping coefficient, k_{ij} is the spring constant and $F(t)$ is the impact force. The initial conditions are

$$U_1(0) = U_2(0) = U_3(0) = U_4(0) = U_5(0) = 0 \quad (2a)$$

$$\dot{U}_1(0) = \dot{U}_2(0) = \dot{U}_3(0) = \dot{U}_4(0) = \dot{U}_5(0) = V \quad (2b)$$

where V is the initial impact velocity. After the drop table strikes the base table, the drop table, base plate and standoff are immovable. The aftershock displacements for the test board and sample packages can be observed from the base plate where the accelerometer is mounted. Another coordinate system, x is selected to observe the vibration of m_1, m_2 and m_3. The origin of x system is located at the observation surface and u_i is the relative displacements. All the displacements can then be defined as

$$U_i = U_3 + u_i \quad (3)$$

As mentioned earlier, U_3 is the local coordinate system located on the top surface of base plate where the accelerometer is mounted. Notice that gravity is along the negative x-direction. Rewrite Equation (1) and the full equations of the system in x-direction can be expressed as

$$\begin{bmatrix} m_1 & 0 & 0 & 0 & 0 \\ 0 & m_2 & 0 & 0 & 0 \\ 0 & 0 & m_3 & 0 & 0 \\ 0 & 0 & 0 & m_4 & 0 \\ 0 & 0 & 0 & 0 & m_5 \end{bmatrix} \begin{Bmatrix} \ddot{U}_3 + \ddot{u}_1 \\ \ddot{U}_3 + \ddot{u}_2 \\ \ddot{U}_3 \\ \ddot{U}_3 + \ddot{u}_4 \\ \ddot{U}_3 + \ddot{u}_5 \end{Bmatrix} +$$

$$\begin{bmatrix} c_{12} & -c_{12} & 0 & 0 & 0 \\ -c_{12} & c_{12}+c_{23} & -c_{23} & 0 & 0 \\ 0 & -c_{23} & c_{23}+c_{34} & -c_{34} & 0 \\ 0 & 0 & -c_{34} & c_{34}+c_{45} & -c_{45} \\ 0 & 0 & 0 & -c_{45} & c_{45} \end{bmatrix} \begin{Bmatrix} \dot{U}_3 + \dot{u}_1 \\ \dot{U}_3 + \dot{u}_2 \\ \dot{U}_3 \\ \dot{U}_3 + \dot{u}_4 \\ \dot{U}_3 + \dot{u}_5 \end{Bmatrix} +$$

$$\begin{bmatrix} k_{12} & -k_{12} & 0 & 0 & 0 \\ -k_{12} & k_{12}+k_{23} & -k_{23} & 0 & 0 \\ 0 & -k_{23} & k_{23}+k_{34} & -k_{34} & 0 \\ 0 & 0 & -k_{34} & k_{34}+k_{45} & -k_{45} \\ 0 & 0 & 0 & -k_{45} & k_{45} \end{bmatrix} \begin{Bmatrix} U_3+u_1 \\ U_3+u_2 \\ U_3 \\ U_3+u_4 \\ U_3+u_5 \end{Bmatrix} = \begin{Bmatrix} 0 \\ 0 \\ 0 \\ 0 \\ F(t) \end{Bmatrix} \quad (4)$$

Rearrange Equation (4) to

$$\begin{bmatrix} m_1 & 0 & 0 & 0 & 0 \\ 0 & m_2 & 0 & 0 & 0 \\ 0 & 0 & m_3 & 0 & 0 \\ 0 & 0 & 0 & m_4 & 0 \\ 0 & 0 & 0 & 0 & m_5 \end{bmatrix} \begin{Bmatrix} \ddot{u}_1 \\ \ddot{u}_2 \\ \ddot{u}_3 \\ \ddot{u}_4 \\ \ddot{u}_5 \end{Bmatrix} +$$

$$\begin{bmatrix} c_{12} & -c_{12} & 0 & 0 & 0 \\ -c_{12} & c_{12}+c_{23} & -c_{23} & 0 & 0 \\ 0 & -c_{23} & c_{23}+c_{34} & -c_{34} & 0 \\ 0 & 0 & -c_{34} & c_{34}+c_{45} & -c_{45} \\ 0 & 0 & 0 & -c_{45} & c_{45} \end{bmatrix} \begin{Bmatrix} \dot{u}_1 \\ \dot{u}_2 \\ \dot{u}_3 \\ \dot{u}_4 \\ \dot{u}_5 \end{Bmatrix} +$$

$$\begin{bmatrix} k_{12} & -k_{12} & 0 & 0 & 0 \\ -k_{12} & k_{12}+k_{23} & -k_{23} & 0 & 0 \\ 0 & -k_{23} & k_{23}+k_{34} & -k_{34} & 0 \\ 0 & 0 & -k_{34} & k_{34}+k_{45} & -k_{45} \\ 0 & 0 & 0 & -k_{45} & k_{45} \end{bmatrix} \begin{Bmatrix} u_1 \\ u_2 \\ u_3 \\ u_4 \\ u_5 \end{Bmatrix} = \begin{Bmatrix} -m_1\ddot{U}_3 \\ -m_2\ddot{U}_3 \\ -m_3\ddot{U}_3 \\ -m_4\ddot{U}_3 \\ -m_5\ddot{U}_3 + F(t) \end{Bmatrix} \quad (5)$$

However, the aftershock relative displacements remains only between m_1 and m_2, and between m_2 and m_3, respectively. The board level drop test system can then be separated as two independent structure and Equation (5) can then be rewritten in two independent equations as

$$\begin{bmatrix} m_1 & 0 \\ 0 & m_2 \end{bmatrix} \begin{Bmatrix} \ddot{u}_1 \\ \ddot{u}_2 \end{Bmatrix} + \begin{bmatrix} c_{12} & -c_{12} \\ -c_{12} & c_{12}+c_{23} \end{bmatrix} \begin{Bmatrix} \dot{u}_1 \\ \dot{u}_2 \end{Bmatrix} +$$

$$\begin{bmatrix} k_{12} & -k_{12} \\ -k_{12} & k_{12}+k_{23} \end{bmatrix} \begin{Bmatrix} u_1 \\ u_2 \end{Bmatrix} = \begin{Bmatrix} -m_1\ddot{U}_3 \\ -m_2\ddot{U}_3 \end{Bmatrix} \quad (6a)$$

$$\begin{bmatrix} m_4 & 0 \\ 0 & m_5 \end{bmatrix} \begin{Bmatrix} \ddot{u}_4 \\ \ddot{u}_5 \end{Bmatrix} + \begin{bmatrix} c_{34}+c_{45} & -c_{45} \\ -c_{45} & c_{45} \end{bmatrix} \begin{Bmatrix} \dot{u}_4 \\ \dot{u}_5 \end{Bmatrix} +$$

$$\begin{bmatrix} k_{34}+k_{45} & -k_{45} \\ -k_{45} & k_{45} \end{bmatrix} \begin{Bmatrix} u_4 \\ u_5 \end{Bmatrix} = \begin{Bmatrix} -m_4\ddot{U}_3 \\ -m_5\ddot{U}_3 + F(t) \end{Bmatrix} \quad (6b)$$

The initial conditions for drop test board with sample packages in Equation (6a) are

$$u_1(0) = u_2(0) = \dot{u}_1(0) = \dot{u}_2(0) \quad (7a)$$

The initial conditions for drop table and base plate in

Equation (6b) are

$$u_4(0) = u_5(0) = \dot{u}_4(0) = \dot{u}_5(0) \quad (7b)$$

In FIG. 3, the acceleration is defined as

$$G(t) = G_m \sin(\frac{\pi t}{T}) \quad (8)$$

The velocity and displacement are derived as follow

$$V(t) = \int G(t)dt = \int_0^t G_m \sin(\frac{\pi\tau}{T})d\tau = G_m \frac{T}{\pi}(1-\cos(\frac{\pi t}{T})) \quad (9)$$

$$D(t) = \int V(t)dt = \int_0^t G_m \frac{T}{\pi}(1-\cos(\frac{\pi\tau}{T}))d\tau$$

$$= G_m \frac{T}{\pi}(t - \frac{T}{\pi}\sin(\frac{\pi t}{T})) \quad (10)$$

In this research, G_m is 1500G and T is 0.0005s. Equation (6a) – (10) can be easily applied to the finite element model of board level drop impact test.

Finite Element Model

Finite element modeling based on ANSYS for a board-level test vehicle subjected to JEDEC drop test standard JESD22-B110 is revealed in this section. A strip finite element model sliced from the entire system is applied to satisfy the support excitation scheme. In order to save the computational time and remain the accuracy, submodelling technique around the interested solder joint is modeled.

Strip Model

Fifteen of 3D pyramid stack die POP package were mounted on the 132 mm x 77mm test board shown in FIG. 4 to study solder joint reliability on the dynamic drop effects in this study. Preliminary results show the maximum bending deflection which is found in the region near sample U_8. This would imply the maximum amplitude occurred in this area and the peak effective stress on solder joint is reported. Thus, a sliced strip model is selected and applied to evaluate

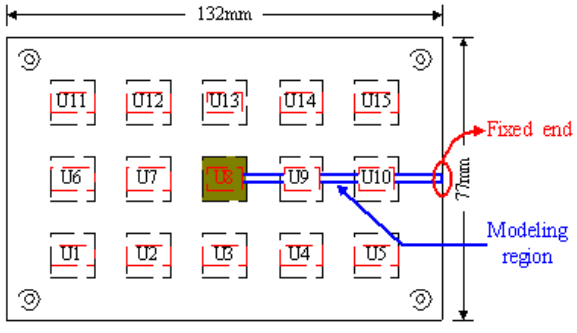

FIG. 4 STRIP MODEL SLICED FROM THE ENTIRE TEST BOARD

the dynamic impact effects. FIG. 5 shows the finite element meshed strip model with boundary conditions for drop impact evaluation. FIG. 6 displays finite element 2D meshed strip model. Detailed dimensions of POP package used in this study are listed in TABLE 1.

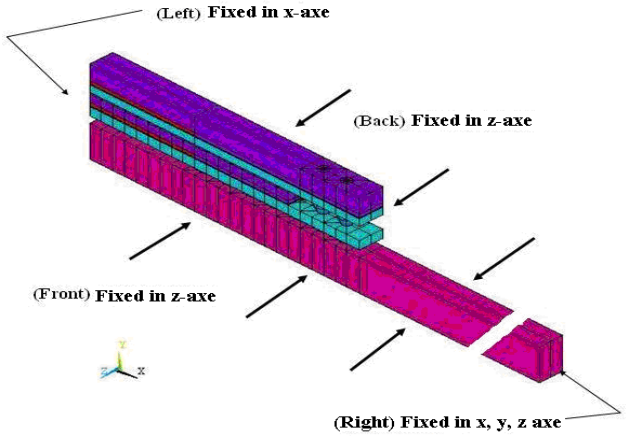

FIG. 5 FINITE ELEMENT STRIP MODEL WITH BOUNDARY CONDITION FOR DROP TEST

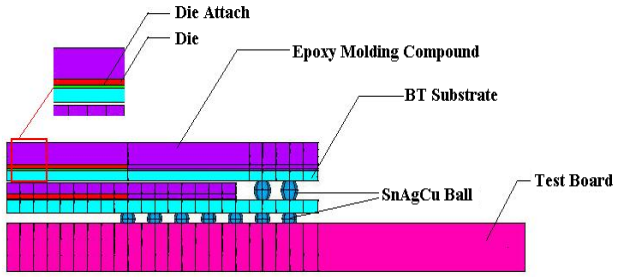

FIG. 6 FINITE ELEMENT MESHED MODEL (2D FRONT VIEW)

TABLE 1 DIMENSIONS OF POP PACKAGE USED IN THIS STUDY

PoP Package	Dimensions
Die Size	6 mm x 6mm
Die Thickness	4 mil
Package Size	15 mm x 15mm
Die Attach Thickness	1 mil
Bottom Compound Thickness	0.35 mm
Upper Compound Thickness	0.45 mm
Bottom Substrate Thickness	0.26 mm
Upper Substrate Thickness	0.21 mm

(note: 1 mil=0.0254 mm)

Material Property

TABLE 2 and TABLE 3 show the material properties for selected SnAgCu (SAC) alloys as well as polymeric materials used in this study. It should be noted that E is the Young's modulus, ν is the Poisson's ratio, ρ is

the density and *G* is the shear modulus.

TABLE 2 MATERIAL PROPERTIES USED IN THIS STUDY

Material	E(GPa)	ν	ρ (g/cm3)
Substrate/Test Board	Transversely Isotropic(Refer to Table 3)		1.91
Sn4.0Ag0.5Cu	43	0.3	8.42
Sn3.5Ag0.5Cu	52	0.36	7.44
Sn3.5Ag	46	0.3	7.39
Die	131	0.23	2.33
Die Attach	2.7	0.35	3.15
Compound	28	0.35	1.89

TABLE 3 TRANSVERSELY ISOTROPIC MATERIAL PROPERTY OF SUBSTRATE AND TEST BOARD

E_x, E_y (GPa)	E_z (GPa)	G_{xz}, G_{yz} (GPa)	G_{xy} (GPa)	ν_{xz}, ν_{yz}	ν_{xy}
16.8	7.4	7.59	3.31	0.39	0.11

All the components are assumed linearly elastic except the solder joints. The material behavior of solder joints should reflect its large impact deformation at very high strain rate. Elastic-plastic tensile mechanical properties for selected SAC alloys were measured and the true stress-strain curves were illustrated in FIG. 7. Multilinear kinematic hardening (MKIN) material model is taken into account the effects of time-independent plasticity behavior when the solder ball suffers bending and dynamic phenomena.

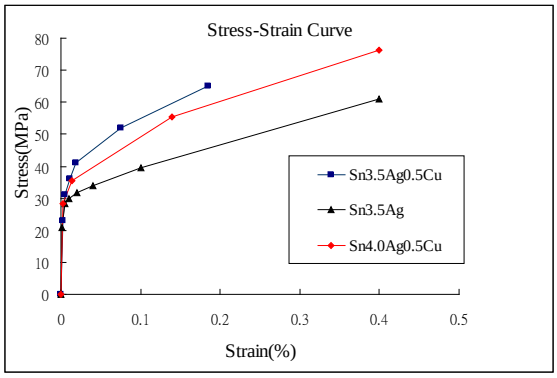

FIG. 7 ELASTIC-PLASTIC TENSILE MECHANICAL BEHAVIOR FOR SAC ALLOYS

Damping coefficients in Equation (6) can be formed by Rayleigh damping matrix

$$[c] = \alpha[m] + \beta[k] \tag{11}$$

where $[m]$ is the mass matrix and $[k]$ is the stiffness matrix. The coefficients of α and β are set to be 0.1 and 0.1 in ANSYS.

Submodel Technique

Based on St. Venant's principle, the cut-boundary interpolation displacement method from coarse model is applied to obtain the results for the small interesting area. FIG. 8 presents the sliced strip coarse model and submodel of outermost solder ball off the end. FIG. 9 illustrates the enlarged view of outermost solder ball in the submodel. In order to examine the potential fracturing area, the top surface of solder ball refers to the package side, while the bottom surface is referring to the test board side.

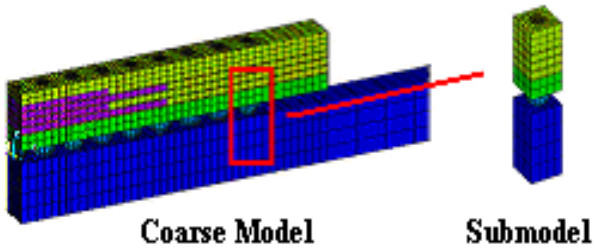

FIG. 8 FINITE ELEMENT COARSE MODEL AND INTERESTED SUBMODEL

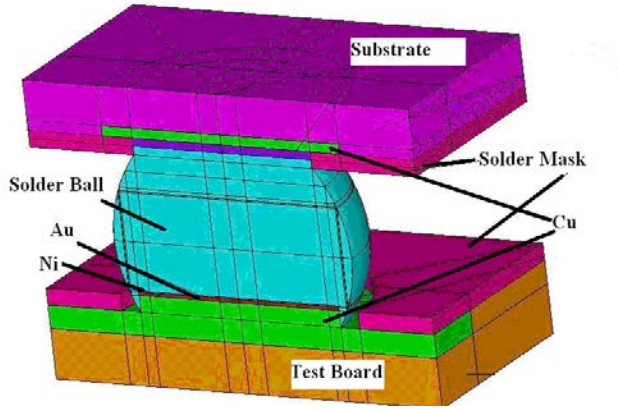

FIG. 9 ENLARGED VIEW OF MAPPED MESH OF SOLDER BALL

Results and Discussion

Finite Element Analysis

A general purpose software ANSYS based on finite element method is utilized to predict the dynamic drop impact reliability of SnAgCu alloy solder balls. Sn4Ag0.5Cu alloy was first applied to the material model to study mesh density and the stressed area on the solder ball. The predicted peak von Mise's stressed area was found in the lower level, the outermost solder ball where plastic failure was reported. FIG. 10 demonstrates the enveloped von Mise's stress contours on the solder balls from center to the outermost along the strip model.

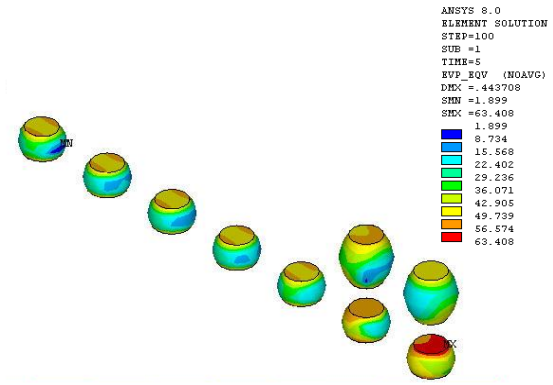

FIG. 10 ENVELOPED VON MISE'S STRESS CONTOURS ON THE SOLDER BALLS

FIG. 11 illustrates the change of vibration amplitude at the maximum stressed observation point. Obviously the hilltop of the first amplitude is around 1.87 mm (downward) at 0.8 ms aftershock. In the second amplitude, the hilltop is around 1.23 mm (upward) at 2.25 ms. However, the oscillation tends to return to the position of equilibrium, i.e. amplitude becomes zero due to the effect of Rayleigh damping. FIG. 12 presents the response von Mise's stress without time-independent plasticity behavior at the outermost solder ball. As it can be seen, von Mise's stress exceeds the elastic region in the first oscillation. Thus, the effect of time-independent plasticity behavior needs to be included in the material model.

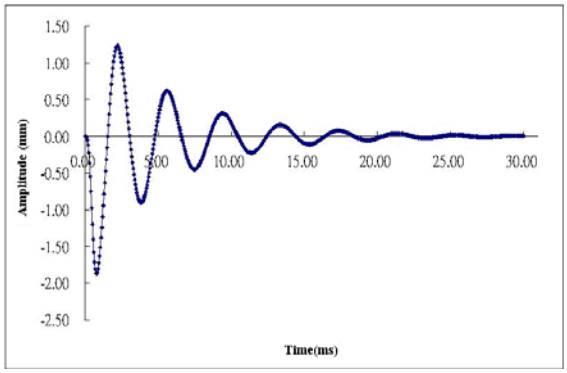

FIG. 11 PREDICTED AMPLITUDE VS. TIME AT THE OUTERMOST SOLDER BALL

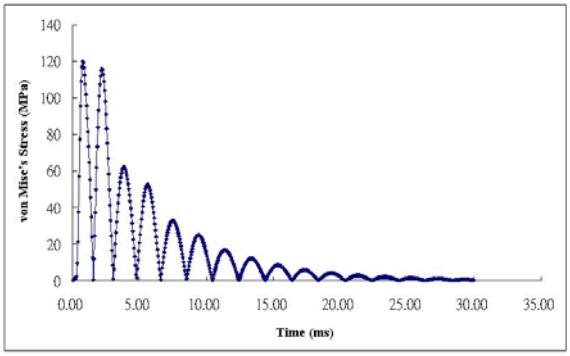

FIG. 12 PREDICTED VON MISE'S STRESS AT THE OUTERMOST SOLDER BALL

Submodel Technique

Since the peak effective stress is located at the outmost solder ball in the lower level, it is of interest to evaluate the location of potential fracture in the outermost solder ball. The enveloped equivalent stress contours for coarse model (strip model) and submodel (outermost solder joint) were observed. The peak equivalent stress is found to be 79.4 Mpa in sliced coarse model, 74.22 MPa (688 elements) and 72.218 MPa (17424 elements) in submodel. Comparison of coarse model and submodel is listed in TABLE 4.

TABLE 4 COMPARISON OF COARSE MODEL AND SUBMODEL.

Finite Element Model	CPU Time (hr)	Effective Stress (MPa)	HD Storage (GB)
Coarse model (162120 elements)	44.3	79.4	45.8
Submodel (688 elements)	1.4	74.22	9.8
Submodel (17424 elements)	11.2	72.218	17.6

FIG. 13 demonstrates the predicted von Mise's stress contours on the region near substrate side (top) and the peak von Mise's stress is 63.394 MPa. However, predicted peak von Mise's stress is 74.22 MPa in FIG. 14, which implies that the potential plastic failure would occur near test board side (bottom).

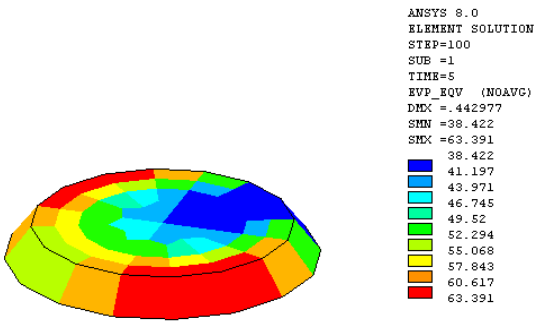

FIG. 13 PREDICTED VON MISE'S STRESS CONTOURS ON THE REGION NEAR SUBSTRATE SIDE (TOP)

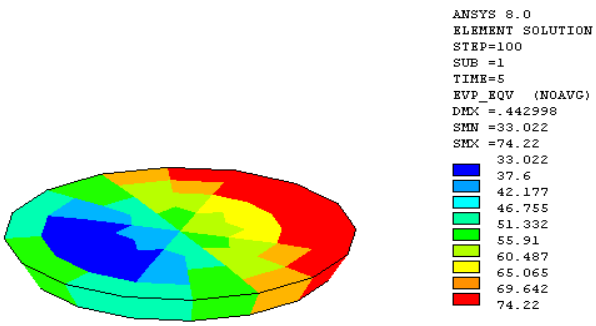

FIG. 14 PREDICTED VON MISE'S STRESS CONTOURS ON THE REGION NEAR TEST BOARD SIDE (BOTTOM)

Lead-free Material

Lead-free SnAgCu solder alloys have been widely used in the IC package industry in recent years. In this study, Sn4Ag0.5Cu, Sn3.5Ag0.5Cu and Sn3.5Ag alloys are introduced to study the effect of lead-free solder on drop impact response. TABLE 5 lists the predicted peak amplitude and the predicted maximum effective stress during drop test. For Sn3.5Ag0.5Cu and Sn3.5Ag, solder ball without copper is much more flexible. For Sn4Ag0.5Cu and Sn3.5Ag0.5Cu, an increase in the weight percentage of silver (Ag) in the solder ball will result in a slightly increase in the amplitude.

TABLE 5 PREDICTED AFTERSHOCK RESPONSE FOR DIFFERENT LEAD-FREE SOLDER ALLOYS

Material	Sn4Ag0.5Cu	Sn3.5Ag0.5Cu	Sn3.5Ag
Predicted Amplitude (mm)	1.87	1.84	2.03
Predicted Effective Strain (%)	0.189	0.185	0.24
Predicted Effective Stress (MPa)	76.4	65	61.4

Conclusions

This paper demonstrates an insight into the plastic failure mechanism associated with dynamic drop impact analysis. Finite element predictions reveal the potential fracture region at the outermost solder joint in the lower level off the end of the strip model. Based on parametric studies in this study, some conclusions have been summarized as follows:

1. The envelope equivalent stress profile has been reached maximum at the outermost solder joint in the lower level in the strip model.

2. The peak equivalent stress, located at the surface near the test board side, implies that the solder fracturing initially occurs at this region.

3. The reliability of Sn4.0Ag0.5Cu and Sn3.5Ag0.5Cu alloys show the peak effective stress would be decreased as the ingredient of Ag decreases in the solder, which implies solder joint can absorb more heavy impact distortion energy as tin (Sn) is increased.

4. For Sn3.5Ag0.5Cu and Sn3.5Ag alloys, the peak effective stress increases as the ingredient of copper (Cu) increases in the solder, i.e. SnAgCu alloys has better reliability.

5. For structure analysis, an increasing in the thickness of molding compound or a decreasing in the height of test board will produce a lower peak effective stress and improve the reliability of solder joints.

6. An increase in the height of solder ball results in a larger deformation on the solder ball which is threatening the structure of solder ball.

ACKNOWLEDGMENT

The authors would like to express their appreciation to the National Science Council (NSC-99-2221-E-214-012 and NSC100-2221-E-214-034) in Taiwan, R.O.C. for financial support.

REFERENCES

Chen, Z. H., Wang, X. F., Liu, Y. and Liu, S., "Drop test simulation of 3D stacked-die packaging with Input-G finite element method," Proc. 11th ICEPT-HDP, pp. 742-746, Xi'an, China, (2010).

Hsu, H. C., Hsu, Y. C., Lee, H. Y., Yeh, C. L. and Lai, Y. S., "Finite Element Prediction of Stack-Die Packages under Board Level Drop Test," Material Science Forum, 594 (2006): 169-174.

Hsu, H. C., Hsu, Y. C., Lee, H. Y., Yeh, C. L. and Lai, Y. S., "Application of Submodeling Technique to Transient Drop Impact Analysis of Board-level Stacked Die Packages," Proc. 8th EPTC, Singapore, pp.412-418, (2006).

Jenq, S. T., Sheu, H. S., Yeh, C. L., Lai, Y. S. and Wu, J. D., "High-G drop impact response and failure analysis of a chip packaged printed circuit board," International Journal of Impact Engineering, 34 (2007): 1655-1667.

Lai, Y. S., Yang, P. F., Yeh, C. L. and Kung, H. Y., "Board-level Reliability of Chipscale Packages Subjected to JEDEC Drop Test Condition," Proc. IMAPS Taiwan Technical Symposium, pp.50-55, (2005).

Lee, Y. C., Wang, B. T., Lai, Y. S., Yeh, C. L. and Chen, R. S., "Finite element model verification for packaged printed circuit board by experimental modal analysis," Microelectronics Reliability, 48 (2008):1837-1846.

Lee, Y. J., Su, Y. F., Hung, T. Y. and Chiang, K. N., "Reliability Analysis of 3D IC Integration packaging under Drop Test Condition," Proc. IMPACT 2012, pp. 654-660, Taipei, Taiwan, (2012).

Pang, J. H. L., Low, K. H., Xiong, B. S. and Che, F. X., "Design for Reliability (DFR) Methodology for

electronic Packaging Assemblies," Proc. 5th EPTC, Singapore, pp.470-478, (2003).

Sakuma, K., Sueoka, K., Kohara, S., Matsumoto, K., Noma, H., Aoki, T., Oyama, Y., Nishiwaki, H., Andry, P. S., Tsang, C. K., Knickerbocker, J. U. and Orii, Y., "IMC Bonding for 3D Interconnection," Proc. 60th ECTC, pp. 864-871, Las Vegas, USA, (2010).

Syed, A., Lin, W., Sohn, E. S. and Cha, S. W., "Plastic deformation and life prediction of solder joints for mechanical shock and drop/impact loading conditions," Proc. 57th ECTC, pp. 507-514, Reno, USA, (2007).

Tee, T. Y., Ng, H. S., Lim, C. T., Pek, E. and Zhong, Z., "Impact Life Prediction Modeling of TFBGA Packages under Board Level Drop Test," Microelectronics Reliability, 44(7), (2005): 1131-1142.

Tsai, T. Y., Yeh, C. L., Lai, Y. S. and Chen, R. S., "Nonlinear Transient Submodeling Analysis for Board-level Drop Test," Proc. IMAPS Taiwan Technical Symposium, pp.185-193, (2006).

Tummala, R. R., "SOP: What is it and why? A new micro system-integration technology paradigm-Moore's law for system integration of miniaturized convergent systems of the next decade," IEEE Transactions on Advanced Packaging, 27(2004):241-249.

Wang, Y. Y., Wang, F. and Chai, T. C., "Finite Element Modeling of CSP Packages Subjected to Board Level Drop Test," Proc. 6th EPTC, Singapore, pp.684-688, (2004).

Wiese, S. and Rzepka, S., "Time-independent Elastic-Plastic Behaviour of Solder Materials," Microelectronics Reliability, 44(12), (2006): 1893-1900.

Hsiang-Chen Hsu received the Ph.D. degree in mechanical engineering from North Carolina State University (Raleigh), USA, in 1993. He is currently a full professor in the Department of Mechanical and Automation Engineering, I-Shou University, Taiwan, R.O.C. His research interests include reliability design and structural analysis in semiconductor packaging, design and fabrication on microfluidic Bio-MEMS sensor, micro/nano tribology.

Shen-Wen Ju received his B.Sc. degree from the Department of Mechatronic Engineering of Huafan University, Taiwan in 2005, and his M.Sc. degree from the Department of Mechanical and Automation Engineering of I-Shou University, Taiwan, R.O.C., in 2007. Currently, he is a senior R&D engineer in Avantpac IC Packaging Company in Kaohsiung City, Taiwan.

Shih-Jeh Wu received his Ph.D. degree from the department of Mechanical Engineering of the Penn. State university (University Park) USA in 1996. He is currently an Assistant Professor in the Department of Mechanical and Automation Engineering, I-Shou University, Taiwan, R.O.C. His research interests include non-destructive evaluation, Laser micromachining applications, and bioengineering.

Miinshyan Bair received Ph.D. degree in Electrical Engineering Department from the University of Manchester UK in 1994. He is currently a joined associate professor in the Department of Media Design and the Department of Electronic Engineering, I-Shou University, R.O.C. His research interests include Digital image processing, medical imaging, process control, capacitance tomography and digital multimedia applications.